THE JOURNAL OF PHYSICAL CHEMISTRY B
A JOURNAL OF THE AMERICAN CHEMICAL SOCIETY

pubs.acs.org/JPCB

Article

Selective Recognition of Phosphatidylinositol Phosphate Receptors by C-Terminal Tail of Mitotic Kinesin-like Protein 2 (MKlp2)

Hyunhyuk Tae,[§] Soohyun Park,[§] Seong-Oh Kim, Saziye Yorulmaz Avsar, and Nam-Joon Cho*

Cite This: *J. Phys. Chem. B* 2022, 126, 2345−2352

Read Online

ACCESS | Metrics & More | Article Recommendations | Supporting Information

ABSTRACT: The mitotic kinesin-like protein 2 (MKlp2) plays a key role in the proper completion of cytokinetic abscission. Specifically, the C-terminal tail of MKlp2 (CTM peptides) offers a stable tethering on the plasma membrane and microtubule cytoskeleton in the midbody during abscission. However, little is known about the underlying mechanism of how the CTM peptides bind to the plasma membrane of the intercellular bridge. Herein, we identify the specific molecular interaction between the CTM peptides and phosphatidylinositol phosphate (PIP) receptors using quartz crystal microbalance-dissipation and atomic force microscopy force spectroscopic measurements. To systematically examine the effects of amino acids, we designed a series of synthetic 33-mer peptides derived from the wild-type (CTM1). First, we evaluated the peptide binding amount caused by electrostatic interactions based on 100% zwitterionic and 30% negatively charged model membranes, whereby the nonspecific attractions were nearly proportional to the net charge of peptides. Upon incubating with PIP-containing model membranes, the wild-type CTM1 and its truncated mutation showed significant PI(3)P-specific binding, which was evidenced by a 15-fold higher binding mass and 6-fold stronger adhesion force compared to other negatively charged membranes. The extent of the specific binding was predominantly dependent on the existence of S21, whereby substitution or deletion of S21 significantly hindered the binding affinity. Taken together, our findings based on a correlative measurement platform enabled the quantification of the nonelectrostatic, selective binding interactions of the C-terminal of MKlp2 to certain PIP receptors and contributed to understanding the molecular mechanisms on complete cytokinetic abscission in cells.

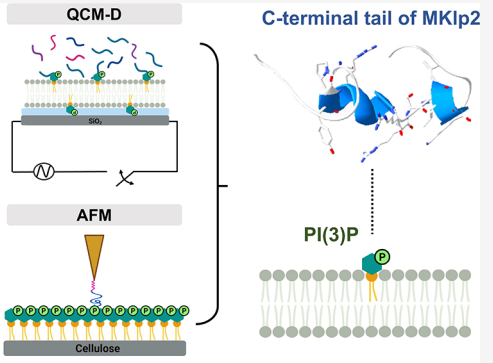

INTRODUCTION

Cytokinesis, a physical process dividing the cytoplasm of the parental cell into two daughter cells after segregation of the genetic material, is a crucial process to finish cell division.[1−3] During the cytokinesis, chromosomal passengers such as Aurora B kinase coordinate the mitotic events, mediating metaphase chromosome alignment and spindle assembly checkpoint signaling.[4−6] In the last phase of cytokinesis, Aurora B plays a key role in abscission, which occurs by splitting apart the plasma membrane in the intercellular bridge and midbody.[7,8] Within these pathways, the mitotic kinesin-like protein 2 (MKlp2), as well as Aurora B, is an essential regulator that contributes to the spatiotemporal recruitment of Aurora B to the central spindle, the intracellular bridge between dividing cells.[9−11] Specifically, MKlp2 anchors to the plasma membrane and/or Flemming body in the intercellular bridge via the C-terminus, and phosphorylation of MKlp2 by Aurora B controls the timing of the abscission process.[12−14] As Aurora B is a member of the serine/threonine protein kinases, the binding between MKlp2 and the plasma membrane involves phosphorylation of serine, specifically at S878, in the C-terminus of MKlp2.[5,15−17] The phosphorylated MKlp2 inhibits the binding to the plasma membrane and arrests cells at the abscission stage,[12] which emphasizes the importance of the binding mechanism of MKlp2 to the plasma membrane in the abscission process.

One mechanism for binding proteins to the plasma membrane is their interaction with phosphoinositides.[18] Phosphoinositides are acidic membrane lipids, which are able to be seven phosphatidylinositol phosphate (PIP) variants by phosphorylation of hydroxyl groups on the positions of 3, 4, and 5 in the inositol head group reversibly.[19] They are enriched in the plasma membrane of the intercellular bridge and participate in mitosis/cytokinesis by recruiting PIP-binding proteins.[8,20] For example, phosphatidylinositol 3-phosphate (PI(3)P) accumulates in the midbody and has important functions on abscission in cytokinesis, such as the contribution to the ANCHR (Abscission/NoCut checkpoint regulator; ZFYVE19) function or localization for regulation of abscission timing.[7,21,22] In another case, phosphatidylinositol

Received: December 13, 2021
Revised: February 23, 2022
Published: March 22, 2022

https://doi.org/10.1021/acs.jpcb.1c10534
J. Phys. Chem. B 2022, 126, 2345−2352

A

CTM	Sequences
1: Wild-Type	P T C Q S S T D C S P Y A R I L R S R R S P L L K S G P F G K K Y
2: S21E	P T C Q S S T D C S P Y A R I L R S R R E P L L K S G P F G K K Y
3: Y12E/S21E	P T C Q S S T D C S P E A R I L R S R R E P L L K S G P F G K K Y
4: S21J	P T C Q S S T D C S P Y A R I L R S R R J P L L K S G P F G K K Y
5: P11A/Y12A/R14A/P22A/L23A/L24A/K25A	P T C Q S S T D C S A A A A I L R S R R S A A A A S G P F G K K Y
6: 1–23	P T C Q S S T D C S P Y A R I L R S R R S P L
7: 1–13	P T C Q S S T D C S P Y A

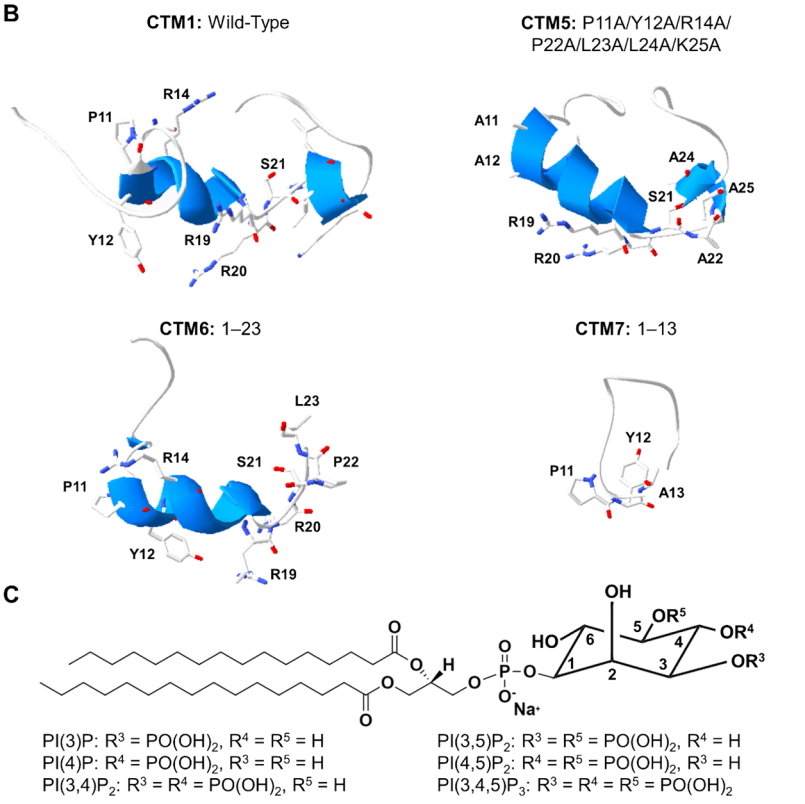

Figure 1. Peptides derived from MKlp2 and molecular structures of PIPs used in this study. (A) Series of amino acid sequences of peptides related to C-terminal tail of MKlp2 (CTM peptide). The 33-mer wild type, CTM1, was used as a template for other variants (CTM2−7) to assess the interaction between peptides and PIP receptors. The highlighted gray regions denote the basic P·X·X·R/K residues. The amino acid J in CTM4 indicates phosphorylated serine. (B) Modeled peptides' secondary structures by the PEP-FOLD online server.[31] The helical conformation was shown in a ribbon representation. (C) General structure of PIP molecules used in the study.

4,5-bisphosphate ($PI(4,5)P_2$) provides specific binding of ERM (ezrin, radixin, and moesin) proteins on the plasma membrane and controls ERM activation, which is necessary for proper spindle orientation in cytokinesis.[23] Likewise, many functional proteins in cytokinesis anchor to the plasma membrane by specific binding to PIPs.[22,24] Since the C-terminal tail of MKlp2 offers stable tethering of MKlp2 to the plasma membrane and microtubule cytoskeleton in the midbody, this motif might selectively bind to PIPs essential to abscission in cytokinesis. However, the detailed mechanism of the molecular interaction that underlies these phenomena remains elusive.

Here, we identified the specific molecular interaction between the C-terminal tail of MKlp2 (termed CTM peptides) and PIP molecules via biophysical approaches. To investigate the interactions between them, a PIP-containing model membrane was fabricated through a solvent-assisted lipid bilayer (SALB) method, and a series of synthetic peptides corresponding to the wild-type CTM peptide (labeled CTM1) and various permutations (CTM2−7) were designed. We first utilized quartz crystal microbalance-dissipation (QCM-D) monitoring to characterize the effects of electrostatic interactions between CTM peptides and the negatively charged lipid bilayer. Then, the binding affinity of CTM peptides on the PIP-containing lipid bilayer was monitored in real time by QCM-D. Furthermore, atomic force microscopy (AFM) force spectroscopic measurements were performed for characterizing quantitative adhesion force and deciphering the molecular mechanisms between CTM peptides and PIP molecules.

EXPERIMENTAL SECTION

Reagents. High-purity CTM peptides were synthesized by AnaSpec Corporation (Fremont, CA, USA). The lyophilized peptide was weighed and solubilized in deionized water to prepare a highly concentrated stock solution (2 mg/mL). The 1,2-dioleoylsn-glycero-3-phosphocholine (DOPC) and 1,2-dioleoyl-*sn*-glycero-3-phospho-(1′-rac-glycerol) (sodium salt)

https://doi.org/10.1021/acs.jpcb.1c10534
J. Phys. Chem. B 2022, 126, 2345−2352

(DOPG) were purchased in lyophilized powder form from Avanti Polar Lipids (Alabaster, AL). Phosphatidylinositol 3-phosphate diC16 (PI(3)P), PI(4)P, PI(3,4)P_2, PI(3,5)P_2, PI(4,5)P_2, and PI(3,4,5)P_3 were obtained from Echelon Biosciences (Salt Lake City, UT).

Physicochemical Properties of CTM Peptides. The isoelectric point and hydrophobicity of CTM peptides were analyzed with Prot pi Peptide Tool (https://www.protpi.ch/Calculator/PeptideTool). Specific phosphorylation of S21 in CTM4 was set for the peptides, with "local" modifications and the applicable location. The default parameters were set to calculate the isoelectric point of peptides, and the net charge of peptides was calculated at pH 7.4.

Quartz Crystal Microbalance-Dissipation Measurements. The SALB formation method was used to prepare supported lipid bilayers (SLBs) for QCM-D measurements.[25] Briefly, an appropriate amount of lipids was dissolved in chloroform and mixed in a glass vial. Then, the chloroform solvent was evaporated with nitrogen gas, forming a dry lipid film on the walls of the glass vial. The lipid film was stored overnight in a vacuum desiccator to remove trace residues of chloroform. Then, the lipid film was dissolved in isopropanol followed by dilution to 0.5 mg/mL right before the experiment. A Q-Sense E4 (Biolin Scientific AB, Gothenburg, Sweden) instrument was employed to monitor the adsorption kinetics of lipids onto silicon oxide AT-cut piezoelectric quartz crystals. Changes in frequency (Δf) and energy dissipation (ΔD) were recorded as a function of time. The measurement data was collected at the $n = 3-11$ overtones, and the reported values were recorded at the third overtone. All samples were introduced at a flow rate of 50 μL/min using a peristaltic pump (Reglo Digital, Ismatec, Glattbrugg, Switzerland) under continuous flow conditions. The temperature of the flow cell was fixed at 25.0 ± 0.5 °C. Before the experiment, sensor surfaces were treated with oxygen plasma (PDC-002, Harrick Plasma, Ithaca, NY) at 180 W for 1 min immediately before use.

Force Spectroscopic Measurements. The cantilevers were rectangular-shaped with single-crystal silicon (CSG-01, NT-MDT, Moscow, Russia), and the normal spring constant was ~0.03 N/m to measure the peptide and lipid membrane binding interaction. The probe tip was used as-supplied and was coated with a 3 nm-thick adhesion layer of titanium. The 35 nm-thick gold layer was then followed to be utilized in the later step of functionalization. The functionalization method was reported in a previous study.[26] Briefly, the gold-coated tips were treated with ethanol, dried with nitrogen gas, and were subjected to oxygen plasma treatment (PSD-UV Benchtop UV−ozone cleaner, Novascan, Ames, IA). Immediately after the plasma treatment, the tips were incubated in 10 mM 2-aminoethanethiol in ethanol for 6 h. After incubation, the tips were washed with ethanol, dried with a stream of nitrogen gas, and immersed in toluene solution with 1 mM NHS-PEG_{24}-MAL for 6 h. Then, the functionalized tips were rinsed and were incubated overnight in a PBS containing 52 μM respective CTM peptides. The force spectroscopic measurements were performed on a commercial AFM instrument (NX-Bio, Park Systems, Suwon, South Korea). The approach and retract speeds of the AFM cantilever were 2000 nm/s with a maximum loading force of 3 nN. For force curve analysis, data organization was conducted by the use of the XEI v1.8.2 software program (Park Systems), and calculation of the adhesion force was done with a custom-written script in Python (available upon request). Zero separation indicates the point of contact between CTM peptides and PIP receptors when the peptide-tethered probe approaches the membrane surface for molecular adhesion events. The piezo displacement was converted to 0 nm of separation distance when the probe first contacts the membrane surface during the approach.

RESULTS AND DISCUSSION

Peptide Design Rationale. Clusters of positively charged amino acids in signaling and cytoskeleton proteins often localize to the negatively charged plasma membranes including PIP molecules mainly by electrostatic interactions.[27,28] Likewise, the wild-type CTM peptide contains a series of basic amino acids (R/K) for the potential function of plasma membrane bindings. Those include three repetitive P·X·X·R/K motifs[12] as gray-shaded entries in Figure 1. In addition, the localization of Aurora B/PP2A by MKlp2 and the phosphorylation of MKlp2, which has been known to happen at Y869 and S878, are essential regulators that provide the targeting of MKlp2 to the plasma membrane and abscission controlling.[9,11,12,29,30]

Therefore, based on the primary structure analysis of MKlp2, we designed various mutations of CTM peptides based on the wild-type sequence to investigate the molecular interactions between CTM peptides and PIP lipids (Figure 1A). The nonconservative mutations were carried out in two directions that might affect molecular interactions: phosphorylation/phosphomimetic substitution and inhibition of the basic amino acid clusters. CTM1 is the wild-type 33-mer peptide (P1 to Y33), originally from P858 to Y890 of MKlp2. As the phosphorylation takes place on Y869 (Y12) and S878 (S21), our synthetic mutations started from silencing the function of one or both residues. For example, the phosphomimetic substitution of S21 with glutamate (CTM2), the substitutions of both Y12 and S21 with glutamate (CTM3), and the substitution of S21 with phosphorylated serine (J21, CTM4) are among them. The CTM2−4 exhibited predicted hydrophobicity similar to CTM1, with a slightly lower net charge due to the negative charge of glutamate or phosphorylated serine (Table S1). In order to break the clusters of basic amino acids, CTM5 was designed by substituting two basic P·X·X·R/K motifs with alanine clusters. Lastly, the truncated forms of CTM6 and CTM7 were defined by removing the last 10 and 20 amino acids, respectively, from the C-terminal end of CTM1. CTM5−7 represented the blocking of two or three basic clusters in CTM1, showing a low predicted net charge depending on the degree of blockages.

Figure 1B presents the prediction of the CTM peptide's secondary structure by the PEP-FOLD online server.[31] The predicted secondary structure of CTM1 exhibited two partial helices connected with random-coil conformation, whereby its substituted mutations, CTM2−4, showed almost identical predictions (data are not shown). The disruption of basic clusters by alanine (CTM5) also showed a similar structure as its wild-type, CTM1, by demonstrating two distinct helices starting from the 11th and from the 22nd amino acid position, which are the beginning of basic P·X·X·R/K motifs in the original sequence. As expected, a single helical structure was obtained from the truncation of the second basic motifs (CTM6), whereas a dominant random coil structure was observed in CTM7 with a complete deletion of basic motifs.

https://doi.org/10.1021/acs.jpcb.1c10534
J. Phys. Chem. B 2022, 126, 2345−2352

In order to unravel which position of phosphate(s) might be able to cause a specific interaction, six types of PIPs were studied to screen their effects. PIP molecules consist of diacylglycerol and carbohydrate moieties via phosphodiester linkage and are categorized by the phosphorylated positions and numbers in the carbohydrate inositol ring (Figure 1C). The phosphate groups in the inositol ring grant PIP molecules negative charges at physiological pH, often leading to specific binding of proteins and PIP molecules based on the multivalent interactions including electrostatic attraction.[32−34]

Electrostatic Interaction between CTM Peptides and Negatively Charged Lipid Membranes. The conventional vesicle fusion method can be limited to fabricate biologically applicable SLBs due to the highly negative charge and/or curvature effect from lipids.[35] Previously, we developed the SALB method as a useful tool to fabricate SLBs for biological applications to complement the drawback of the vesicle fusion method, as demonstrated by SLB formation composed of highly anionic DOPG[36] and PIP lipids.[37] In the SALB method, the phospholipid molecules undergo a series of phase transitions from inverted micelles and/or monomers to micelles and lamellar nanostructures as the solvent is exchanged from an organic solvent to aqueous solution, resulting in the formation of SLBs with numerous types of phospholipids and/or sterols.[25,38] Accordingly, we utilized the SALB method in this study to fabricate various SLBs containing a high proportion of negatively charged lipids and PIP molecules.

In Figure S1, the SLB fabrication steps monitored by QCM-D are presented. The first step involves (i) the injection of isopropanol after stabilization of the baseline signal in aqueous buffer solutions followed by (ii) the addition of the lipid mixture in isopropanol and (iii) the solvent exchange to aqueous buffer. Once the signal stabilizes, the final values of the resonance frequency shift (Δf) and energy dissipation shift (ΔD) were collected to verify whether the SLB was successfully formed. Furthermore, the quality of SLB was assessed by measuring the adsorption amount of bovine serum albumin (BSA), whereby high-quality SLBs are resistant to nonspecific adsorption of proteins, unlike the bare silicon dioxide surfaces. All fabricated SLBs went through the BSA adsorption process to ensure the complete coverage of the surface to prevent the nonspecific adsorption of peptides in the later step. Nevertheless, our fabricated SLBs showed negligible adsorption of BSA (Figure S1C), indicating that a complete, fully covered SLB was formed on the crystal surface.

We first evaluated the effects of electrostatic charge on the interaction between CTM peptides and lipid membranes by comparing the 100 mol % zwitterionic lipid (DOPC) and 30 mol % negatively charged lipid (DOPG) mixed with 70 mol % DOPC compositions (Figure 2A). In QCM-D measurements, the changes in resonance frequency (Δf) and energy dissipation (ΔD) reflect the mass and viscoelastic properties of the adsorbed layers, respectively. After the formation of complete SLBs with the respective compositions, 25 μM CTM peptides were introduced on the SLBs to determine the amount of bound peptide.

Upon incubation of CTM peptides within the DOPC lipid bilayer, less than 1 Hz shifts were observed from most of the CTM peptides, indicating that the nonspecific interactions between CTM peptides and the zwitterionic DOPC lipid membrane were negligible (Figure 2B). On the contrary, CTM1−4 demonstrated 3−10 Hz shifts against highly

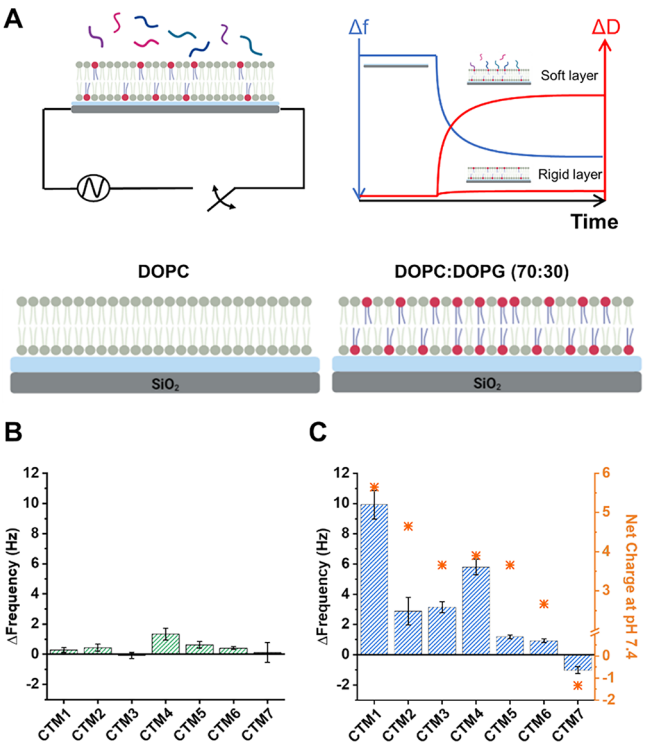

Figure 2. QCM-D monitoring of the CTM peptide interaction with zwitterionic and negatively charged lipid bilayer platforms. (A) Schematic representation of the QCM-D technique to measure the real-time binding kinetics of CTM peptides onto respective SLBs. The changes in resonance frequency and energy dissipation reflect the mass and viscoelastic properties of the bound peptide, respectively. In order to assess the influence of electrostatic charge, the SLBs made of 100 mol % zwitterionic lipid, DOPC, and 30 mol % negatively charged lipid, DOPG, with 70 mol % DOPC were used. The graphical illustrations were not drawn to scale. Final Δf shift caused by CTM peptides onto (B) DOPC and (C) 30 mol % DOPG with net charge of CTM peptides at pH 7.4. Data are reported as mean ± standard deviation from at least two repeated measurements.

negatively charged membranes (Figure 2C). As the isoelectric point of the wild-type CTM1 is calculated as 10.1, the peptide is cationic (+5.7) at a physiological pH of 7.4. Therefore, the electrostatic attraction seemed to affect the adsorption of CTM1 on negatively charged DOPG lipids. Similarly, CTM2, 3, and 4 exhibited lower Δf shifts because of lower predicted net charges compared to their wild-type CTM1 caused by the substitution of neutral serine and/or tyrosine to negatively charged amino acids such as glutamate or phosphorylated serine. Aside from the electrostatic attraction, the binding affinity of CTM1 by hydrogen bonding from serine appeared to be trivial since the binding was restrained by the phosphorylation of serine, which can still form hydrogen bonding.[39] The trend remained the same in CTM5 and 6 cases, whereby the Δf shifts by peptides were reduced to ∼1 Hz, comparable to the neutral DOPC SLB, attributed to the removal of positively charged amino acids. In contrast, as the predicted net charge of CTM7 was −1.3, the peptide was repelled from the SLB and even showed a decreased mass, which might have been caused by minor disruption of the membranes because of the electrostatic repulsion. In summary, CTM peptides showed a consistent binding behavior to negatively charged membranes nearly proportional to their

https://doi.org/10.1021/acs.jpcb.1c10534
J. Phys. Chem. B 2022, 126, 2345−2352

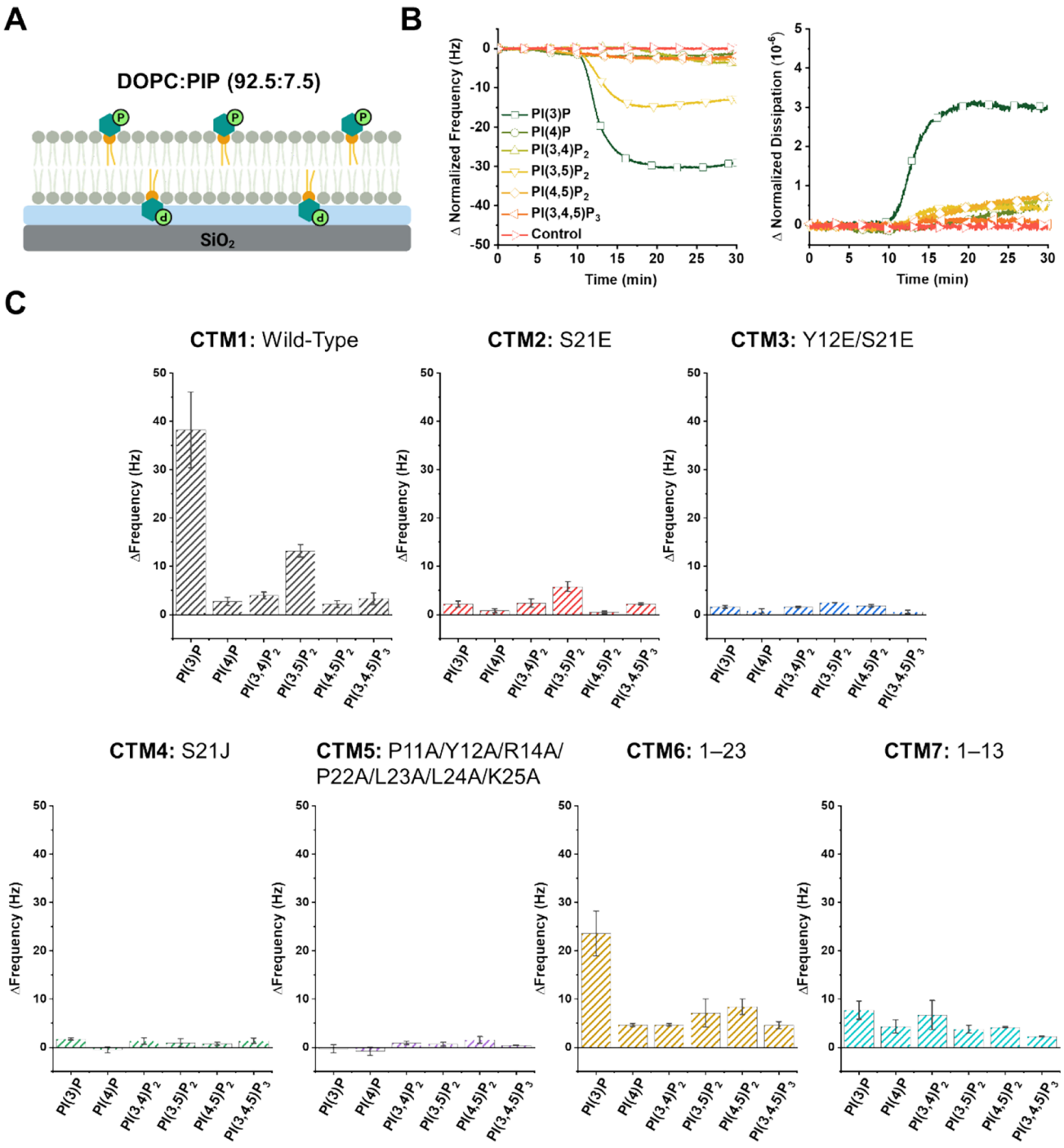

Figure 3. QCM-D evaluation of CTM peptides binding to PIP-containing SLBs. (A) Graphical illustration of the SLB formed with 7.5 mol % PIP receptors and 92.5 mol % DOPC (not drawn to scale). (B) QCM-D response as a function of time for wild-type CTM1 binding to different types of PIP-doped SLBs. The resonance frequency change (Δf, left panel) and energy dissipation (ΔD, right panel) shifts were normalized to 0 at the point where stable SLBs were formed to compare the differences. Peptides were added at t = 10 min. (C) Final Δf shift caused by the respective peptide onto different types of PIP-doped SLBs. Data are reported as mean ± standard deviation from at least two repeated measurements.

predicted net charges, which should be considered while assessing the peptides' binding toward PIP molecules.

Selective Binding of CTM Peptides to Various PIP Receptors. Next, we attempted to determine the selective binding behavior of CTM peptides to different types of PIP-containing lipid membranes. The SLBs doped with 7.5 mol % PIP molecules with 92.5 mol % DOPC were fabricated by the SALB method (Figure 3A). The Δf and ΔD shifts in QCM-D measurements were normalized to 0 at the point where BSA was added in the final step to ensure the complete SLB formation before adding CTM peptides. After injecting of CTM peptides (t = 10 min), the binding dynamics were monitored by Δf and ΔD shifts, whereby some of them show dramatic changes as shown in Figure 3B. The substantial decrease in the resonance frequency indicated an increase in the mass of the surface-adsorbed layer due to the associated CTM peptides with the PIP-laden lipid membrane.

https://doi.org/10.1021/acs.jpcb.1c10534
J. Phys. Chem. B 2022, 126, 2345−2352

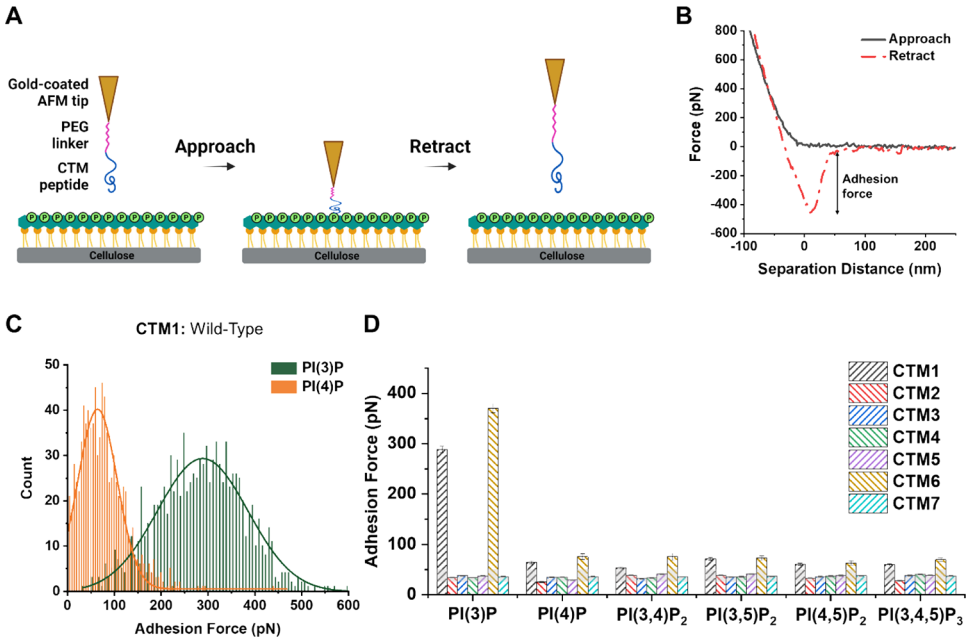

Figure 4. Specificity of the CTM peptide binding to PIP molecules. (A) Schematic representation of AFM force spectroscopic measurements. (B) Representative AFM force−distance curve upon approach and retract for the molecular adhesion event between the wild-type CTM1 and PI(3)P receptor. The loading speed was 2 μm/s. (C) Histogram of individual adhesion events for the wild-type CTM1 binding to different PIP receptors. Here, >500 events were recorded per PIP receptor in independent experiments. (D) Statistical comparison of the most probable adhesion forces between the CTM peptides−PIP interaction calculated by raw data, and the statistical error was estimated as $2.35\sigma/N$, where σ is the standard deviation and N is the number of data set. The gray shade denotes the most probable adhesion force for the control experiment without any peptides.[26]

The total final value of Δf shifts after injection of CTM peptides is presented in Figure 3C. Strikingly, the wild-type CTM1 showed a considerable binding amount of 38.2 Hz to PI(3)P and 13.2 Hz to PI(3,5)P_2, demonstrating ∼3 times higher preference toward PI(3)P rather than PI(3,5)P_2. By contrast, other PIPs with phosphorylation(s) at different ring position(s) showed much less binding amount. Of note, the maximum binding amount that resulted from 30 mol % DOPG was ∼10 Hz with CTM1, which is ∼15-fold less in molar ratio compared to the PIP-embedded membrane considering that the mole fraction of PIP incorporation is four times less (7.5 mol %) than that of the DOPG case. This result indicates that there is a strong specific interaction beyond the electrostatic force between CTM1 and certain PIP receptors such as PI(3)P as well as PI(3,5)P_2.

On the other hand, CTM2, S21 substituted by glutamate, demonstrated a largely reduced binding amount, as in the case where CTM3 and CTM4 showed negligible response to all types of PIP molecules. This implies that the existence of S21 largely affected the binding dynamics of peptides onto the PIP-containing lipid membrane because a phosphomimetic substitution or phosphorylation of S21 blocked most of the specific bindings to PI(3)P. Interestingly, CTM5, the alanine-substituted peptide in the P·X·X·R/K motifs (with intact S21 residue), also lost its activity toward all PIP receptors, inferring that the first two basic motifs might be a prerequisite of PIP interaction. The next result with CTM6, a mutated peptide by truncating the last two basic clusters, offers clearer evidence that the key basic cluster conferring the PIP attraction is the first basic motif because CTM6 exhibited moderate binding to PI(3)P (23.6 Hz), which is only ∼40% reduction compared to the wild-type CTM1. As expected, CTM7, a 13-mer by removing all basic clusters and S21, was unable to bind onto any types of PIP-containing lipid membranes selectively. Although CTM6−7 showed small binding to some PIP receptors, they did not bind properly beyond the electrostatic binding of CTM1, where the binding amount was ∼10 Hz to the negatively charged membrane. It implied that the first basic motif could provide the electrostatic binding but not selective binding between CTM peptides and PIP receptors. To sum up, S21 is one of the primary factors regulating the specific binding to PI(3)P and/or PI(3,5)P_2, whereby the basic P·X·X·R/K motifs, especially the first motif, also largely contribute to a proper binding configuration of CTM peptides.

Adhesion Force Measurement by Atomic Force Microscopy. To further investigate the binding interactions, we performed AFM force spectroscopic measurements that can directly measure the adhesion forces between the peptides and lipid molecules. This quantitative measurement strategy is useful to examine the specificity and strength of the CTM peptides−phosphoinositide interactions.[26] First, the gold-coated AFM probe tip was amine-functionalized to be reacted with PEG linkers exposed with free maleimide ester at the end. Then, the cysteine residue(s) from the CTM peptides was conjugated with a maleimide group to form a stable thioether linkage.[26,40,41] Of note, cysteine residues exist only at the N-terminal of CTM peptides (C3 and C9), ensuring that our target motifs (starting from the basic clusters, P11) were marginally affected by the tethering of peptides to the tip. Next, the PIP-containing monolayers were fabricated on the hydrophobic surface to evaluate the adhesion force between CTM peptides and various PIP receptors (Figure 4A).

A representative force−distance curve of the CTM1−PI(3)P interaction is presented in Figure 4B. During the approach (gray solid line), the peptide-tethered probe goes nearer to contact with the membrane surface at ∼0 nm of separation

https://doi.org/10.1021/acs.jpcb.1c10534
J. Phys. Chem. B 2022, 126, 2345−2352

distance. Then, the force required to break the CTM1−PI(3)P interaction was quantified by a rupture length (∼10 nm) and an adhesion force (420 pN) during the retraction (red dash-dot line). Figure 4C presents the corresponding histograms of individual adhesion force between CTM1 and respective PIP receptors that were obtained from >500 independent rupture events, whereby the most probable adhesion forces were determined by a Gaussian curve fit.[42] For example, the adhesion force of CTM1 against PI(3)P (290 pN) was 4.5 times larger than against PI(4)P (64 pN). Markedly, a previously conducted control measurement without any bound peptides has shown that the most probable adhesion force was ∼40 pN,[26] manifesting that the measured value of the CTM1−PI(4)P interaction is comparable to an untreated probe tip.

Similar to QCM-D measurements, CTM1 and CTM6 showed particularly strong binding to PI(3)P, whereas other mutated peptides showed negligible interactions with other PIP receptors including the ones with similar or higher negative surface charge (Figure 4D). Notably, CTM6 demonstrated ∼85 pN stronger adhesion force than CTM1, which was distinctive from the bound mass result from QCM-D monitoring. This observation might be due to the sensitivity differences of techniques, where QCM-D characterizes the large-scale binding mass of molecules and AFM describes the binding force of molecules at a single-molecular level.[43] Therefore, these biophysical measurements are complementary to each other to analyze the molecular interactions as a whole.

Specific binding between the peptide and PI(3)P can be derived by multiple mechanisms such as conformational binding and hydrophobic interaction. For example, the positively charged small pocket shape (R/K-R/K-H-H-C-R) is suggested for the selective interaction of the FYVE domain with PI(3)P.[44,45] This model also suggests that hydrocarbon chains of PI(3)P interact with the hydrophobic residues in the FYVE domain. Therefore, various biochemical properties of the CTM1 peptide may affect the specific binding to PI(3)P, implying the need for further studies on the explicit mechanisms.

CONCLUSIONS

In this work, we identified the specific molecular interaction between the C-terminal tail motifs of MKlp2 (CTM peptides) and phosphatidylinositol phosphate receptors, particularly PI(3)P, via model membranes and systematic biophysical measurement tools. Using a combination of QCM-D monitoring and AFM force spectroscopic platform, we found that the wild-type, CTM1, and its truncated mutation, CTM6, showed substantial PI(3)P-specific binding beyond electrostatic interactions. The negligible binding of other mutated peptides demonstrates the importance of S21 (originally S878 from MKlp2) and P·X·X·R/K clusters to facilitate high binding specificity of CTM peptides to PI(3)P. Looking forward, our finding offers insight to how MKlp2 specifically binds to the plasma membrane and control the abscission in a molecular level.

ASSOCIATED CONTENT

Supporting Information

The Supporting Information is available free of charge at https://pubs.acs.org/doi/10.1021/acs.jpcb.1c10534.

The physicochemical properties of CTM peptides including relative hydrophobicity (H_R), isoelectric point (pI), and net charge at pH 7.4 (Table S1) and QCM-D frequency shift and dissipation during the formation of PI-containing bilayers on silicon oxide (SiO_2) using the SALB method together with bovine serum albumin (BSA) adsorption onto the bilayer-coated and bare SiO_2 surface (Figure S1) (PDF)

AUTHOR INFORMATION

Corresponding Author

Nam-Joon Cho − *School of Materials Science and Engineering, Nanyang Technological University, 639798, Singapore; China-Singapore International Joint Research Institute (CSIJRI), Guangzhou 510000, China;* orcid.org/0000-0002-8692-8955; Email: njcho@ntu.edu.sg

Authors

Hyunhyuk Tae − *School of Materials Science and Engineering, Nanyang Technological University, 639798, Singapore;* orcid.org/0000-0002-0459-5879

Soohyun Park − *School of Materials Science and Engineering, Nanyang Technological University, 639798, Singapore;* orcid.org/0000-0003-3261-7585

Seong-Oh Kim − *School of Materials Science and Engineering, Nanyang Technological University, 639798, Singapore*

Saziye Yorulmaz Avsar − *School of Materials Science and Engineering, Nanyang Technological University, 639798, Singapore*

Complete contact information is available at: https://pubs.acs.org/10.1021/acs.jpcb.1c10534

Author Contributions

[§]H.T. and S.P. contributed equally to this work

Notes

The authors declare no competing financial interest.

ACKNOWLEDGMENTS

This work was supported by the Ministry of Education (MOE) in Singapore under grant AcRF TIER1-2020-T1-002-032 (RG111/20). This work also supported by the China-Singapore International Joint Research Institute (CSIJRI). Figures [2]A, [3]A, and [4]A were created with BioRender.com. H.T. is supported by an SINGA graduate scholarship from the A*STAR Graduate Academy, Singapore.

REFERENCES

(1) Guertin, D. A.; Trautmann, S.; McCollum, D. Cytokinesis in Eukaryotes. *Microbiol. Mol. Biol. Rev.* **2002**, *66*, 155−178.

(2) Glotzer, M. The Molecular Requirements for Cytokinesis. *Science* **2005**, *307*, 1735−1739.

(3) Pollard, T. D.; O'Shaughnessy, B. Molecular Mechanism of Cytokinesis. *Annu. Rev. Biochem.* **2019**, *88*, 661−689.

(4) Kitagawa, M.; Lee, S. H. The Chromosomal Passenger Complex (Cpc) as a Key Orchestrator of Orderly Mitotic Exit and Cytokinesis. *Front. Cell Dev. Biol.* **2015**, *3*, 14.

(5) Krenn, V.; Musacchio, A. The Aurora B Kinase in Chromosome Bi-Orientation and Spindle Checkpoint Signaling. *Front. Oncol.* **2015**, *5*, 225.

(6) van der Waal, M. S.; Hengeveld, R. C.; van der Horst, A.; Lens, S. M. Cell Division Control by the Chromosomal Passenger Complex. *Exp. Cell Res.* **2012**, *318*, 1407−1420.

(7) Agromayor, M.; Martin-Serrano, J. Knowing When to Cut and Run: Mechanisms That Control Cytokinetic Abscission. *Trends Cell Biol.* **2013**, *23*, 433−441.
(8) Mierzwa, B.; Gerlich, D. W. Cytokinetic Abscission: Molecular Mechanisms and Temporal Control. *Dev. Cell* **2014**, *31*, 525−538.
(9) Gruneberg, U.; Neef, R.; Honda, R.; Nigg, E. A.; Barr, F. A. Relocation of Aurora B from Centromeres to the Central Spindle at the Metaphase to Anaphase Transition Requires Mklp2. *J. Cell Biol.* **2004**, *166*, 167−172.
(10) Adriaans, I. E.; Hooikaas, P. J.; Aher, A.; Vromans, M. J. M.; van Es, R. M.; Grigoriev, I.; Akhmanova, A.; Lens, S. M. A. Mklp2 Is a Motile Kinesin That Transports the Chromosomal Passenger Complex During Anaphase. *Curr. Biol.* **2020**, *30*, 2628−2637.e9.
(11) Hümmer, S.; Mayer, T. U. Cdk1 Negatively Regulates Midzone Localization of the Mitotic Kinesin Mklp2 and the Chromosomal Passenger Complex. *Curr. Biol.* **2009**, *19*, 607−612.
(12) Fung, S. Y. S.; Kitagawa, M.; Liao, P.-J.; Wong, J.; Lee, S. H. Opposing Activities of Aurora B Kinase and B56-Pp2a Phosphatase on Mklp2 Determine Abscission Timing. *Curr. Biol.* **2017**, *27*, 78−86.
(13) Petsalaki, E.; Zachos, G. An Atm−Chk2−Incenp Pathway Activates the Abscission Checkpoint. *J. Cell Biol.* **2021**, *220*, No. e202008029.
(14) Green, R. A.; Paluch, E.; Oegema, K. Cytokinesis in Animal Cells. *Annu. Rev. Cell Dev. Biol.* **2012**, *28*, 29−58.
(15) Tuncel, H.; Shimamoto, F.; Kaneko, H.; Aoki, E.; Jikihara, H.; Nakai, S.; Takata, T.; Tatsuka, M. Nuclear Aurora B and Cytoplasmic Survivin Expression Is Involved in Lymph Node Metastasis of Colorectal Cancer. *Oncol. Lett.* **2012**, *3*, 1109−1114.
(16) Kitagawa, M.; Fung, S. Y. S.; Hameed, U. F. S.; Goto, H.; Inagaki, M.; Lee, S. H. Cdk1 Coordinates Timely Activation of Mklp2 Kinesin with Relocation of the Chromosome Passenger Complex for Cytokinesis. *Cell Rep.* **2014**, *7*, 166−179.
(17) Serena, M.; Bastos, R. N.; Elliott, P. R.; Barr, F. A. Molecular Basis of Mklp2-Dependent Aurora B Transport from Chromatin to the Anaphase Central Spindle. *J. Cell Biol.* **2020**, *219*, No. e201910059.
(18) Jungmichel, S.; Sylvestersen, K. B.; Choudhary, C.; Nguyen, S.; Mann, M.; Nielsen, M. L. Specificity and Commonality of the Phosphoinositide-Binding Proteome Analyzed by Quantitative Mass Spectrometry. *Cell Rep.* **2014**, *6*, 578−591.
(19) Ernest James Phillips, T.; Maguire, E. Phosphoinositides: Roles in the Development of Microglial-Mediated Neuroinflammation and Neurodegeneration. *Front. Cell. Neurosci.* **2021**, *15*, 90.
(20) Echard, A. Phosphoinositides and Cytokinesis: The "Pip" of the Iceberg. *Cytoskeleton* **2012**, *69*, 893−912.
(21) Thoresen, S. B.; Campsteijn, C.; Vietri, M.; Schink, K. O.; Liestøl, K.; Andersen, J. S.; Raiborg, C.; Stenmark, H. Anchr Mediates Aurora-B-Dependent Abscission Checkpoint Control through Retention of Vps4. *Nat. Cell Biol.* **2014**, *16*, 547−557.
(22) Gulluni, F.; Martini, M.; Hirsch, E. Cytokinetic Abscission: Phosphoinositides and ESCRTs Direct the Final Cut. *J. Cell. Biochem.* **2017**, *118*, 3561−3568.
(23) Cauvin, C.; Echard, A. Phosphoinositides: Lipids with Informative Heads and Mastermind Functions in Cell Division. *Biochim. Biophys. Acta, Mol. Cell Biol. Lipids* **2015**, *1851*, 832−843.
(24) Sagona, A. P.; Nezis, I. P.; Pedersen, N. M.; Liestøl, K.; Poulton, J.; Rusten, T. E.; Skotheim, R. I.; Raiborg, C.; Stenmark, H. Ptdins (3) P Controls Cytokinesis through Kif13a-Mediated Recruitment of Fyve-Cent to the Midbody. *Nat. Cell Biol.* **2010**, *12*, 362−371.
(25) Ferhan, A. R.; Yoon, B. K.; Park, S.; Sut, T. N.; Chin, H.; Park, J. H.; Jackman, J. A.; Cho, N.-J. Solvent-Assisted Preparation of Supported Lipid Bilayers. *Nat. Protoc.* **2019**, *14*, 2091−2118.
(26) Kim, S.-O.; Jackman, J. A.; Elazar, M.; Cho, S.-J.; Glenn, J. S.; Cho, N.-J. Quantitative Evaluation of Viral Protein Binding to Phosphoinositide Receptors and Pharmacological Inhibition. *Anal. Chem.* **2017**, *89*, 9742−9750.
(27) Suetsugu, S.; Kurisu, S.; Takenawa, T. Dynamic Shaping of Cellular Membranes by Phospholipids and Membrane-Deforming Proteins. *Physiol. Rev.* **2014**, *94*, 1219−1248.
(28) Heo, W. D.; Inoue, T.; Park, W. S.; Kim, M. L.; Park, B. O.; Wandless, T. J.; Meyer, T. Pi (3, 4, 5) P3 and Pi (4, 5) P2 Lipids Target Proteins with Polybasic Clusters to the Plasma Membrane. *Science* **2006**, *314*, 1458−1461.
(29) Kitagawa, M.; Fung, S. Y. S.; Onishi, N.; Saya, H.; Lee, S. H. Targeting Aurora B to the Equatorial Cortex by Mklp2 Is Required for Cytokinesis. *PLoS One* **2013**, *8*, No. e64826.
(30) Virshup, D. M.; Shenolikar, S. From Promiscuity to Precision: Protein Phosphatases Get a Makeover. *Mol. Cell* **2009**, *33*, 537−545.
(31) Lamiable, A.; Thévenet, P.; Rey, J.; Vavrusa, M.; Derreumaux, P.; Tufféry, P. Pep-Fold3: Faster De Novo Structure Prediction for Linear Peptides in Solution and in Complex. *Nucleic Acids Res.* **2016**, *44*, W449−W454.
(32) Yeagle, P. L. *The Membranes of Cells*; Academic Press, 2016.
(33) Hyvönen, M.; Macias, M. J.; Nilges, M.; Oschkinat, H.; Saraste, M.; Wilmanns, M. Structure of the Binding Site for Inositol Phosphates in a Ph Domain. *EMBO J.* **1995**, *14*, 4676−4685.
(34) Zhao, H.; Hakala, M.; Lappalainen, P. Adf/Cofilin Binds Phosphoinositides in a Multivalent Manner to Act as a Pip2-Density Sensor. *Biophys. J.* **2010**, *98*, 2327−2336.
(35) Jackman, J. A.; Cho, N.-J. Supported Lipid Bilayer Formation: Beyond Vesicle Fusion. *Langmuir* **2020**, *36*, 1387−1400.
(36) Guo, J.; Ho, J. C. S.; Chin, H.; Mark, A. E.; Zhou, C.; Kjelleberg, S.; Liedberg, B.; Parikh, A. N.; Cho, N.-J.; Hinks, J.; Mu, Y.; Seviour, T. Response of Microbial Membranes to Butanol: Interdigitation Vs. Disorder. *Phys. Chem. Chem. Phys.* **2019**, *21*, 11903−11915.
(37) Tabaei, S. R.; Guo, F.; Rutaganira, F. U.; Vafaei, S.; Choong, I.; Shokat, K. M.; Glenn, J. S.; Cho, N.-J. Multistep Compositional Remodeling of Supported Lipid Membranes by Interfacially Active Phosphatidylinositol Kinases. *Anal. Chem.* **2016**, *88*, 5042−5045.
(38) Tabaei, S. R.; Choi, J.-H.; Haw Zan, G.; Zhdanov, V. P.; Cho, N.-J. Solvent-Assisted Lipid Bilayer Formation on Silicon Dioxide and Gold. *Langmuir* **2014**, *30*, 10363−10373.
(39) Mandell, D. J.; Chorny, I.; Groban, E. S.; Wong, S. E.; Levine, E.; Rapp, C. S.; Jacobson, M. P. Strengths of Hydrogen Bonds Involving Phosphorylated Amino Acid Side Chains. *J. Am. Chem. Soc.* **2007**, *129*, 820−827.
(40) Kim, S.-O.; Jackman, J. A.; Mochizuki, M.; Yoon, B. K.; Hayashi, T.; Cho, N.-J. Correlating Single-Molecule and Ensemble-Average Measurements of Peptide Adsorption onto Different Inorganic Materials. *Phys. Chem. Chem. Phys.* **2016**, *18*, 14454−14459.
(41) Mochizuki, M.; Oguchi, M.; Kim, S.-O.; Jackman, J. A.; Ogawa, T.; Lkhamsuren, G.; Cho, N.-J.; Hayashi, T. Quantitative Evaluation of Peptide−Material Interactions by a Force Mapping Method: Guidelines for Surface Modification. *Langmuir* **2015**, *31*, 8006−8012.
(42) Schwesinger, F.; Ros, R.; Strunz, T.; Anselmetti, D.; Güntherodt, H.-J.; Honegger, A.; Jermutus, L.; Tiefenauer, L.; Plückthun, A. Unbinding Forces of Single Antibody-Antigen Complexes Correlate with Their Thermal Dissociation Rates. *Proc. Natl. Acad. Sci. U. S. A.* **2000**, *97*, 9972−9977.
(43) Lebed, K.; Kulik, A. J.; Forró, L.; Lekka, M. Atomic Force Microscopy and Quartz Crystal Microbalance Study of the Lectin-Carbohydrate Interaction Kinetics. *Acta Phys. Pol., A* **2007**, *111*, 273.
(44) Fruman, D. A.; Rameh, L. E.; Cantley, L. C. Phosphoinositide Binding Domains: Embracing 3-Phosphate. *Cell* **1999**, *97*, 817−820.
(45) Misra, S.; Hurley, J. H. Crystal Structure of a Phosphatidylinositol 3-Phosphate-Specific Membrane-Targeting Motif, the Fyve Domain of Vps27p. *Cell* **1999**, *97*, 657−666.

https://doi.org/10.1021/acs.jpcb.1c10534
J. Phys. Chem. B 2022, 126, 2345−2352